Journal of Molecular Structure 1161 (2018) 9–17

Contents lists available at ScienceDirect

Journal of Molecular Structure

journal homepage: http://www.elsevier.com/locate/molstruc

Molecular structure, Hirshfeld surface analysis, theoretical investigations and nonlinear optical properties of a novel crystalline chalcone derivative: (*E*)-1-(5-bromothiophen-2-yl)-3-(*p*-tolyl)prop-2-en-1-one

B. Pramodh [a, 1], N.K. Lokanath [a, *], S. Naveen [b, 1], P. Naresh [c], S. Ganguly [d], J. Panda [e]

[a] Department of Studies in Physics, Manasagangotri, University of Mysore, Mysuru, 570 006, India
[b] Department of Physics, School of Engineering & Technology, Jain University, Bangalore, 562 112, India
[c] GITAM Institute of Pharmacy, GITAM University, Rushikonda, Visakhapatnam, 530 045, India
[d] Department of Pharmaceutical Sciences and Technology, Birla Institute of Technology, Mesra, Ranchi, 835 215, Jharkhand, India
[e] Raghu College of Pharmacy, Dakamarri, Bheemunipatnam, Visakhapatnam, 531 162, India

ARTICLE INFO

Article history:
Received 14 December 2017
Received in revised form
20 January 2018
Accepted 29 January 2018
Available online 14 February 2018

Keywords:
Trigonal planar conformation
π-conjugation
Hirshfeld surface
HOMO-LUMO
MEP
NLO properties

ABSTRACT

In the present work, the crystal structure of a novel chalcone derivative, (*E*)-1-(5-bromothiophen-2-yl)-3-(*p*-tolyl) prop-2-en-1-one has been confirmed by X-ray diffraction studies. Hirshfeld surface analysis was carried out to explore the intermolecular interactions. From the Hirshfeld surface analysis it was observed that H···H (26.7%) and C···H (26.3%) are the major contributors to the intermolecular interactions which stabilizes the crystal structure. The coordinates were optimized using the density functional theory (DFT) calculations using B3LYP hybrid functions with 6-31G(d) basis set. The structural parameters obtained from XRD studies compliment with those calculated using DFT calculations. The HOMO and LUMO energy gap was found to be 4.1778 eV. The molecular electrostatic potential (MEP) was plotted to identify the possible reactions sites of the molecule. Further, non-linear optical (NLO) properties were investigated by calculating hyperpolarizabilities which indicate that the title compound would be a potential candidate for the NLO applications.

1. Introduction

In recent years, organic molecules with delocalized π-electrons have gathered increasing attention due to their potential application in new-generation optical and molecular electronic devices. Therefore, the search for nonlinear optical (NLO) materials with considerable nonlinearities and fast response is essential for technological development. Compared to inorganic conjugates, organic materials have some advantages such as high degree of nonlinearity, low dielectric constants, natural synthetic flexibility and rapid response in opto-electronics filed [1–3]. The electronic properties of the organic materials can be modified by varying the donor/acceptor groups at the end of the parent molecules [4]. Among the organic nonlinear materials, chalcones are well known molecules owing to their interesting applications in biological, pharmaceutical and nonlinear fields. Chalcones exhibit wide range of applications of biology such as anti-inflammatory [5], anti-ulcerative [6], anti-malaria [7], anti-bacterial [8], anti-viral [9] and anti-diabetic activities [10].

Furthermore, Chalcones have a π-conjugated system [11]. Due to overlapping of π orbital, delocalization of electronic charge distributions leads to high mobility of the electron density [12]. The chalcones have been the prime focus of various computational and experimental studies because of their promising applications in various optoelectronics [13,14] and high-speed optical communications [15–17]. The chalcones with high hyperpolaraizabilities are also useful in optical computing and optical communication technologies [18–22].

As a part of our ongoing research on novel chalcones [23–25], herein we describe the properties of chalcone derivative, (*E*)-1-(5-bromothiophen-2-yl)-3-(*p*-tolyl) prop-2-en-1-one. The experimental and theoretical results were compared. Using DFT

* Corresponding author.
E-mail address: lokanath@physics.uni-mysore.ac.in (N.K. Lokanath).
[1] These authors contributed equally.

https://doi.org/10.1016/j.molstruc.2018.01.078
0022-2860/

calculations, non-linear optical properties of the molecule was investigated.

2. Experimental methods

2.1. Synthesis of (E)-1-(5-bromothiophen-2-yl)-3-(p-tolyl) prop-2-en-1-one

The compound was synthesized as per the procedure reported earlier [26]. The reaction mixture was then poured over crushed ice and acidified with dilute HCl and the solid which precipitated was filtered and washed with water, dried and was purified on column chromatography (silica gel with 10% ethyl acetate in hexane). The product was further recrystallized using acetone solvent to obtain good crystals [26]. The spectral characterization, FT-IR spectrum was recorded in the 4000-400 cm^{-1}as KBR pellet on a BRUKER IFS-66V Spectrophotometer, and ^1H NMR spectra was recorded at 400 MHz, in $CDCl_3$, on Bruker 400 MHz Advance III spectrometer. The chemical shifts (δ) are reported in parts per million (ppm) downfield from tetramethylsilane (TMS) as internal reference.

2.2. Single crystal X-ray diffraction studies

X-ray analysis of a suitable single crystal was performed on a Rigaku XtaLABmini CCD diffractometer with X-ray generator operating at 45 kV and 10 mA, using MoK_α radiation of wavelength 0.71073 Å. X-ray intensity data were collected, keeping the scan width of 0.5° and an exposure time of 3 s with the sample to detector distance of 50 mm. A complete data set was processed using Crystal Clear [27,28]. The crystal structure was solved by direct methods and refined by full-matrix least squares method on F^2 using SHELXS and SHELXL programs respectively [29]. All the non-hydrogen atoms were revealed in the first difference Fourier map itself. The geometrical calculations were carried out using the program PLATON [30] and the packing diagrams were generated using Mercury program [31]. Details of the crystal structure and parameters of the final refinement process are summarized in Table 1.

2.3. Computational details

The molecular structure optimization of the molecule and their vibrational harmonic frequencies were calculated using the Density Function Theory (DFT) with Beckee-3-Lee-Yag-Parr (B3LYP) at6-31G (d) basis set using GAUSSIAN09 program [32] package without any constraint on the geometry. Gauss View 05 software [33] was used to visualize the optimized structure. The optimized geometrical parameters, true rotational constants, fundamental vibrational frequencies were calculated. We calibrated the vibrational wavenumbers calculated by B3LYP method. Analytical frequency calculations were carried out to confirm the minimum energy. The Hirshfeld surface analysis was used to explore the molecular interactions using Crystal Explorer program [34]. Further, Density functional theory (DFT) was carried out to examine the ground and excited state properties to obtain the frontier molecular orbitals, highest occupied molecular orbital (HOMO) and lowest unoccupied molecular orbital (LUMO). The molecular electrostatic potential (MEP) surface and density of state have been simulated to find more reactive sites for electrophilic and nucleophilic. The non-linear optical properties such as static dipole moments (μ), mean polarizability ($\langle\alpha\rangle$) and first hyperpolarizabilities (β) have been theoretically computed.

Table 1
Crystal data and structure refinement parameters for the molecule.

Parameter	Compound
CCDC deposit No.	1590163
Empirical formula	$C_{14}H_{11}BrOS$
Formula weight	307.2
Temperature	293 (2) K
Wavelength	MoKα (λ = 0.71073 Å)
Crystal system, space group	Monoclinic $P2_1/a$
Unit cell dimensions	$a = 5.895$ (5) Å $b = 14.105$ (7) Å $c = 15.373$ (8) Å $\alpha = 90.000$ (8)° $\beta = 92.89$ (4)° $\gamma = 90.00$ (4)°
Volume and Z	1276.6 (14) $Å^3$and 4
Density (calculated)	1.598 Mg m^{-3}
Absorption coefficient	3.363 mm^{-1}
F_{000}	616
Crystal size	0.25 × 0.23 × 0.21 mm
θ range for data collection	3.02°to 27.57°
Index ranges	$-7 \le h \le 7$ $-17 \le k \le 17$ $-4 \le l \le 19$
Reflections collected	4752
Independent reflections	2883 [$R_{int} = 0.0660$]
Absorption correction	multi-scan
Refinement method	Full matrix least-squares onF^2
Data/restraints/parameters	2883/0/155
Goodness-of-fit onF^2	0.972
Final [$I > 2\sigma(I)$]	R1 = 0.0525, w$R2$ = 0.1340
R indices (all data)	R1 = 0.0772, w$R2$ = 0.1556
Largest diff. peak and hole	1.701−0.998 e $Å^{-3}$

3. Results and discussions

3.1. Experimental and theoretical FT-IR analysis of compound

The vibrational spectra of (E)-1-(5-bromothiophen-2-yl)-3-(*p*-tolyl) prop-2-en-1-one were simulated to show the presence of functional groups and their vibrational modes. Both experimental and theoretical FT-IR spectra of the molecule confirms the functional groups and the carbonyl stretching vibrations appeared in the region 1750-1660 cm^{-1} [35]. The characteristic vibrational frequencies for the main functional groups are C-$H_{thiophene}$ (Expt. = 3240 cm^{-1} and DFT = 3220 cm^{-1}), C_{sp}2-H (Expt. = 3000 cm^{-1} and DFT = 3120 cm^{-1}), C−H_3 (Expt. = 2866 cm^{-1} and DFT = 3040 cm^{-1}), C=C (Expt. = 1400 cm^{-1} and DFT = 1467 cm^{-1})and C=O (Expt. = 1645 cm^{-1} and DFT = 1710 cm^{-1}). The result reflected a good agreement between the DFT-IR and FT-IR experimental result, as shown in Fig. 1.

3.2. Experimental ^1H NMR compared to theoretical analysis

^1H NMR spectrum of the (E)-1-(5-bromothiophen-2-yl)-3-(*p*-tolyl)prop-2-en-1-one in $CDCl_3$ shows the proposed structural formula (Fig. 2(a)). One broad peak corresponding to the aliphatic CH_3 is seen at 3.40 ppm (experimentally) and 3.35 ppm (theoretically). Several peaks in the aromatic region 7.20−7.90 ppm were attributed to the three CH's of the phenyl and thiophene rings were recorded as shown in Fig. 2(b).

The computed ^1H NMR using NMR-DB software [36] in gaseous state was compared to ^1H NMR in $CDCl_3$ solvent. The correlation coefficient for chemical shifts was found to be 0.9956 as shown in Fig. 2(c).

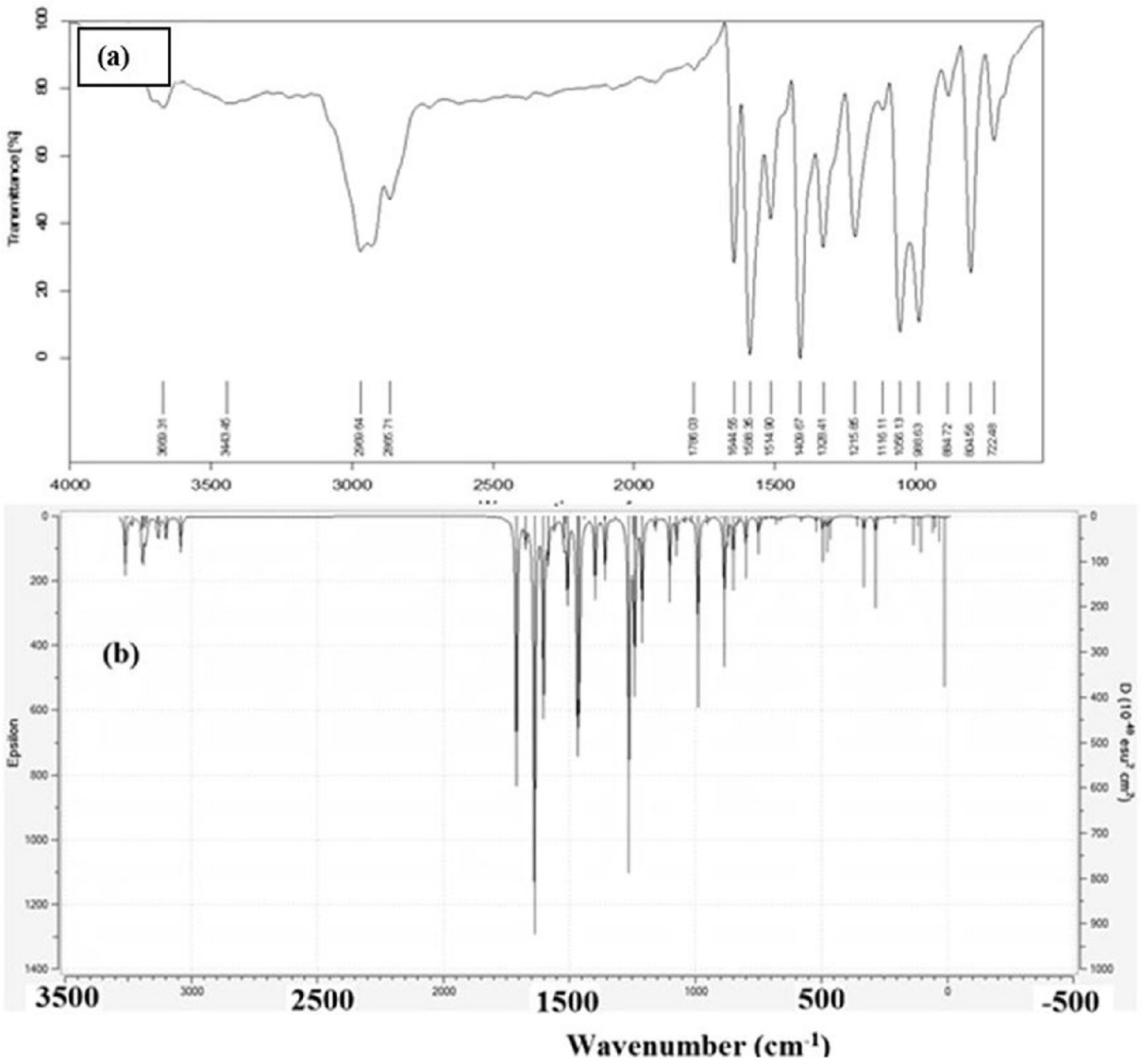

Fig. 1. FT-IR spectra of the molecule obtained by (a) experimental and (b) theoretical calculations by using DFT with B3LYP/6-31G(d) basis set.

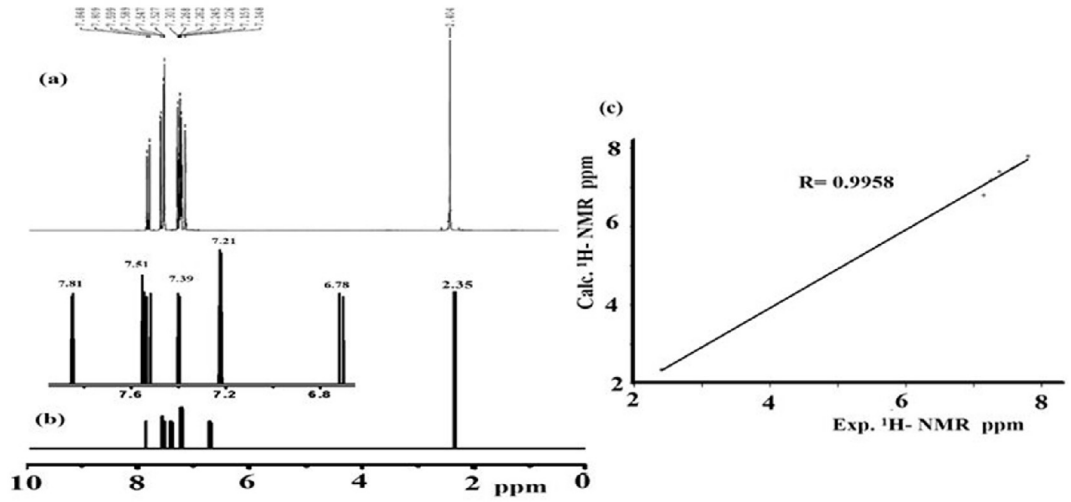

Fig. 2. ^{1}H NMR of (E)-1-(5-bromothiophen-2-yl)-3-(*p*-tolyl)prop-2-en-1-one (a) experimentally with $CDCl_3$, (b) using NMR-DB and (c) Experimental and theoretical comparison of ^{1}H NMR results.

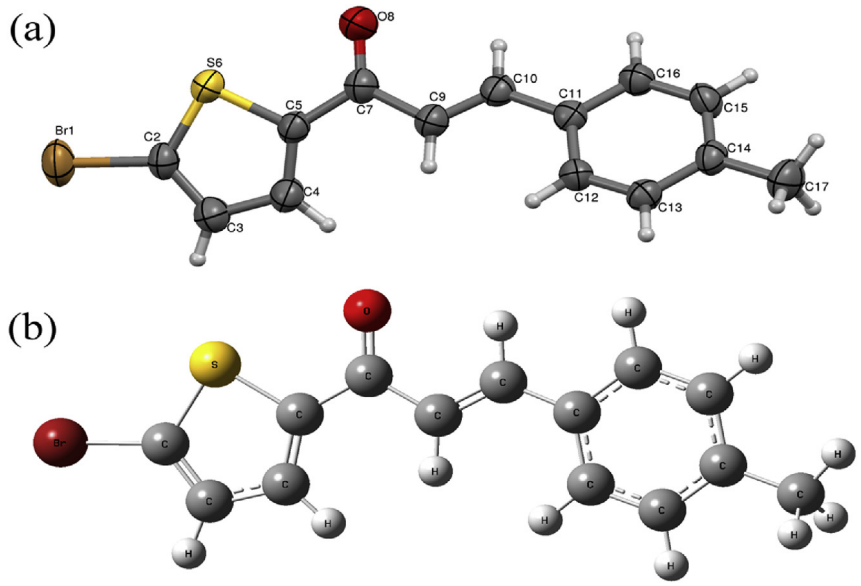

Fig. 3. (a) ORTEP of the molecule with thermal ellipsoids drawn at 50% probability and (b) DFT optimized molecular structure of the title compound.

3.3. Single crystal X-ray diffraction analysis

The details of crystal structure and data refinement parameters are given in Table 1. T the compound crystallizes in monoclinic system with space group $P2_1/a$ with the cell parameters $a = 5.895$ (5) Å, $b = 14.105$ (7) Å, $c = 15.373$ (8) Å and $\beta = 92.89$ (4)°. Fig. 3(a) represents the ORTEP of the molecule with thermal ellipsoids drawn at 50% probability. There are two molecules in an asymmetric unit and they are non-planar. This non-planarity is confirmed by dihedral angles between the thiophene and benzene rings is 41.61 (16) Å. The thiophene ring S atom and enone C=O group are approximately in the same orientation.

The C7 atom [120.01 (3)°, 121.90 (3)° and 118.09 (3)° for O8–C7–C5, O8–C7–C9 and C5–C7–C9, respectively] is in a distorted trigonal planar conformation, which may be due to the steric bulk of the oxygen atom.

The thiophene ring is affected by π-conjugation. This can be explained by the longer C–S bond lengths of 1.697 (3) Å and 1.728 (3) Å for C2–S6 and C5–S6, respectively and the olefinic double bond is in *E*-configuration. The presence of C10–H10···O8 intramolecular hydrogen bond (with D—H = 0.93 Å, H … A = 2.52 Å, D … A = 2.837 Å and D—H … A = 100°) contribute significantly to the

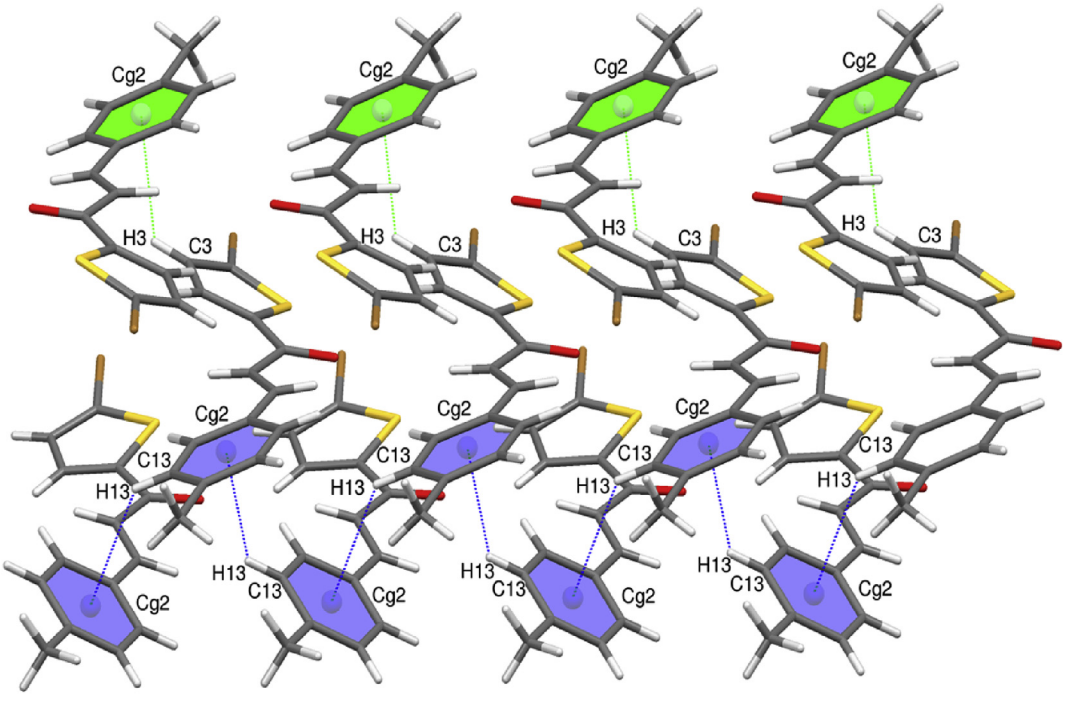

Fig. 4. The packing of the molecule exhibiting zigzag arrangement along the *a*-axis.

Table 2
Comparison of selected bond lengths and bond angles.

Bond lengths (Å)	Expt.	DFT	Bond angles (°)	Expt.	DFT
BR1–C2	1.8770	1.8825	C5–S6–C2	88.59	90.82
S6–C5	1.7280	1.7525	C4–C3–C2	112.42	111.73
S6–C2	1.6970	1.7318	C10–C11–C12	123.54	122.92
O8–C7	1.2240	1.2358	C11–C10–C9	127.96	128.02
C3–C4	1.4090	1.4199	C11–C16–C15	121.19	121.90
C3–C2	1.3550	1.3719	C12–C13–C14	121.24	121.17
C17–C14	1.5048	1.5090	C16–C15–C14	120.95	121.24
C4–C5	1.3520	1.3799	C11–C12–C13	120.89	121.21
C11–C10	1.4627	1.4602	C17–C14–C13	120.67	120.57
C11–C16	1.3843	1.4112	C17–C14–C15	121.32	121.90
C11–C12	1.4010	1.4126	S6–C5–C4	111.09	111.51
C10–C9	1.3113	1.3614	S6–C5–C7	117.29	118.10
C16–C15	1.3866	1.3901	Br1–C2–S6	120.02	119.97
C9–C7	1.4804	1.4704	Br1–C2–C3	126.52	127.10
C13–C12	1.3710	1.3890	S6–C2–C3	113.48	113.37
C13–C14	1.4095	1.4017	O8–C7–C5	122.12	121.89
C15–C14	1.3790	1.4028	O8–C7–C5	119.65	120.00
C5–C7	1.4668	1.4805	C9–C7–C5	118.23	118.18

stabilization of the crystal.

The C–H … π interaction plays a prominent role in stabilizing the crystal structure. The C3–H3 … Cg2 interaction (where Cg2 is centroid of the benzene ring consist of an atoms C11/C12/C13/C14/C15/C16) with C—Cg distance of 3.484 (5) Å, H—Cg distance of 2.96 Å and C–H … Cg angle of 133°(symmetry code *1-x, -y, 1-z*). The C13–H13 … Cg2 interaction with C—Cg distance of 3.569 (5) Å, H—Cg distance of 2.89 Å and C–H … Cg angle of 131°(with symmetry code *1-x, -y, 1-z*). The C13–H13 … Cg2 interaction with C—Cg distance (symmetry code *1/2 + x, 1/2-y, z*) which connect the molecules in a zigzag patterns along *a*-axis as shown in Fig. 4.

The C–H··· π and π—π interactions contribute to the stability of the crystal packing while weak and strong hydrogen bond interactions such as C–H···O, C–H···Br, and C–H···S help to stabilize the molecular structure by forming a three-dimensional network.

3.4. Optimized structure

Theoretical studies have been performed to compare the geometric parameters with those obtained from X-ray diffraction studies. The bond lengths and bond angles corresponding to the optimized geometry of the molecule have been obtained by using the density function theory with B3LYP/6-31G(d) basis set. The optimized geometry of the compound is illustrated in Fig. 3(b).

The selected bond lengths and bond angles are listed in Table 2 along with the experimental data with the correlation coefficient $R^2 = 0.9915$ for bond lengths and $R^2 = 0.9961$ for bond angles are shown in Fig. 5.

4. Theoretical calculations

4.1. Hirshfeld surface analysis

The Hirshfeld surface analysis is used to explore the packing modes, intermolecular interactions and molecular shapes in a crystalline environment (shown in Fig. 6). The Hirshfeld surfaces are mapped with d_{norm} and 2D fingerprint plots presented in this paper were generated using Crystal Explorer 2.1. The spherical atom electron densities were used to calculate the electron distribution based on which the molecular Hirshfeld surfaces in the crystal structure were constructed. The normalized contact distance (d_{norm}) based on both d_e (distance from the point to the nearest nucleus external to the surface) and d_i (distance to the nearest nucleus internal to the surface), and the *vdw* radii of the atom, given by

$$d_{norm} = \frac{d_i - r_i^{vdw}}{r_i^{vdw}} + \frac{d_e - r_e^{vdw}}{r_e^{vdw}}$$

The above equation helps to identify the regions of particular importance to intermolecular interactions [37]. The 2D fingerprint plot provides the summary of intermolecular contacts in the crystal by the combination of d_e and d_i. Shaped-index surfaces are specified on the basis of local curvature of the Hirshfeld surface [38] shown in Fig. 7.

The red concave region on shape index is the acceptor and the blue region is the donor atoms. The dark-red spots on the d_{norm} surface arise as a result of the short interatomic contacts such as strong hydrogen bonds. The adjacent red-blue indicates the C–H … π staking interactions over the surface.

Finger plots in Fig. 7 indicate the relative contributions to the Hirshfeld surface (in %) and difference between intermolecular interaction patterns. The H–H and C–H bonding appears to be major contributors in crystal packing.

4.2. Frontier molecular orbitals (HOMO-LUMO) analysis

The intramolecular charge transfer process from a donor to acceptor moiety of molecular system is usually characterized by the excitation of an electron from occupied orbital (HOMO) to unoccupied orbital (LUMO) and explained by quantum chemical method

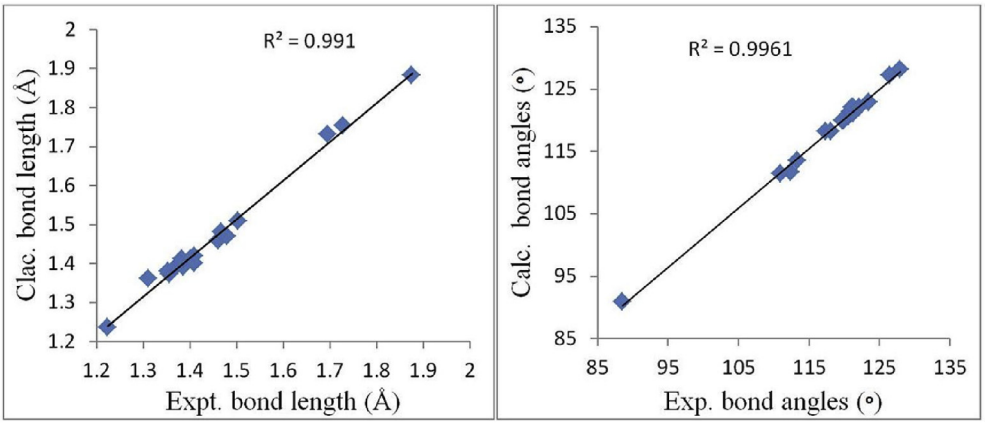

Fig. 5. Correlations between the experimental and calculated bond lengths (Å) and angles (°).

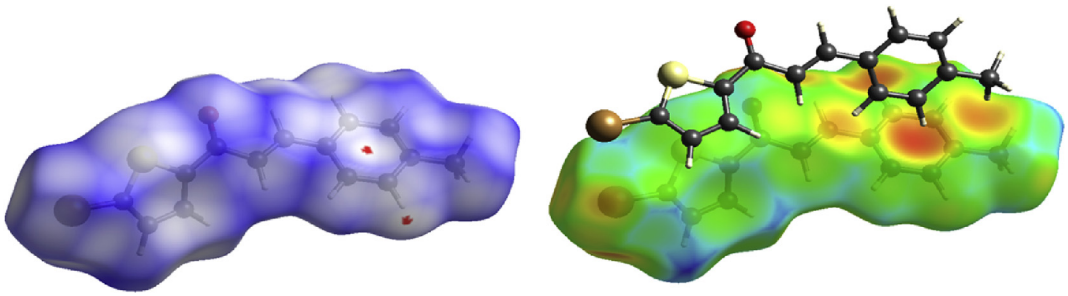

Fig. 6. The Hirshfeld surface mapped wit d_{norm} and shaped index of the title compound.

approach [39]. The intermolecular charge transfer of the title compound molecular orbitals is shown in Fig. 8. The calculated HOMO and LUMO energy gap (ΔE), ionization potential (IP), electron affinity (EA), chemical potential(μ), global hardness (η), softness (σ) and electrophilicity index (ω) of the compound molecule have been computed using B3LYP/6-31G(d) level and are listed in Table 3.

The obtained energy values are in atomic units (a.u.) and those values have been converted into electron volt (eV) by making use of the conversion factors as 1 a. u. = 27.211 eV. It could be seen from the plots that the HOMO (E = −6.2522) levels were spread over the entire molecule except for CH_3 group in excited state. The LUMO (E = −2.1044) of first excited state was almost uniformly distributed over the molecule. The energy gap (ΔE = 4.1478 eV) of HOMO-LUMO explained the eventual charge transfer interaction within the molecule, which reflected the chemical activity of the molecule.

4.3. Molecular electrostatic potential analysis

The molecular electrostatic potential (MEP) analysis can be regarded as a powerful tool for identifying the possible interaction sites around a molecule [40,41]. One of the most interesting features of quantum chemistry is the ability to explain the reactivity of compounds under investigation. It determines the reactivity of a chemical system by predicting electrophilic as well as nucleophilic sites in target molecules [42,43]. Mathematically, MEP can be defined as

$$V(r) = \sum (Z_A/R_{A-r}) - \int \rho(r')/r' - dr'$$

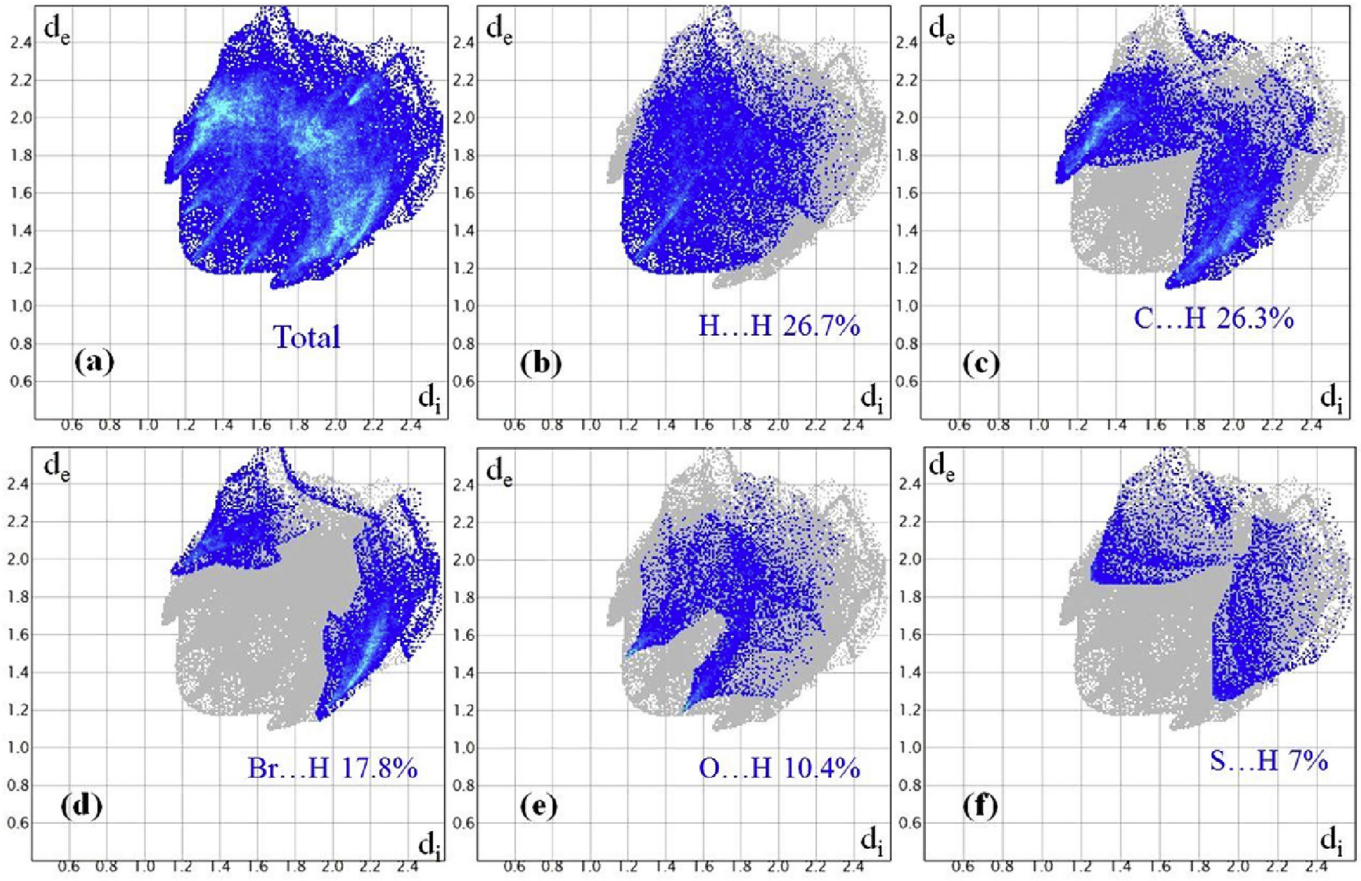

Fig. 7. 2D Finger print plots of the title compound showing individual molecular interactions.

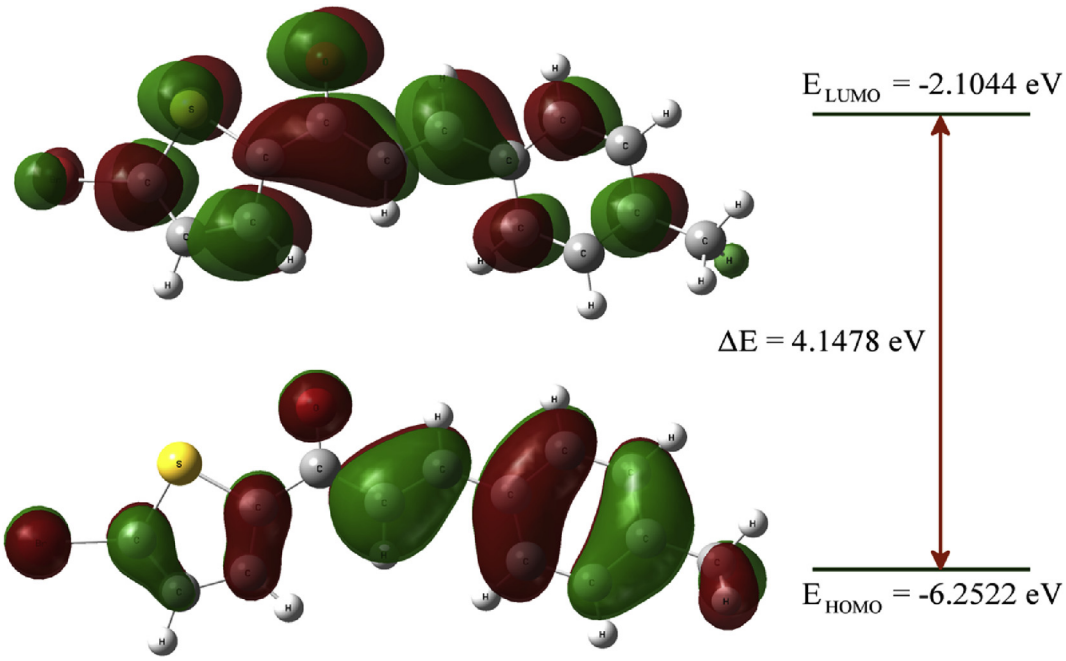

Fig. 8. The molecular orbitals of the title compound.

Table 3
The HOMO and LUMO energy gap, ionization potential, electron affinity, chemical hardness, electronegativity, softness, chemical potential, global electrophilicity index values at the B3LYP/6-31G(d) and B3LYP/6-31G (d,p) level.

Parameter	B3LYP/6-31G(d)	B3LYP/6-31G (d,p)
E_{HOMO} (eV)	−6.2522	−6.2582
E_{LUMO} (eV)	−2.1044	−2.1129
Energy gap (ΔE) (eV)	4.1478	4.1453
Ionization Potential (IP) (eV)	6.2522	6.2582
Electron affinity (EA) (eV)	2.1044	2.1129
Global Hardness (η) (eV)	2.0739	2.0726
Global Softness(σ) (eV^{-1})	0.4821	0.4824
Chemical potential (μ) (eV)	−4.1783	−4.1855
Global Electrophilicity (ω) (eV)	4.2090	4.2262

Summation (Σ) runs over all nuclei, ZA is charge of nucleus which is located at RA and ρ(r') is electron density. The computed MEP using B3LYP/6-31G(d) level of DFT is shown in Fig. 9. The MEP surface allows us to visualize the various charged regions of a molecule. The charge distribution helps to determine the molecules interaction and the nature of chemical bond. The positive area of the MEP is a nucleophilic site, while negative region is associated with an electrophilic site. The Fig. 9 shows the negative charges are more and they are concentrated around the oxygen atom. The color code of the map is in the range between $-6.409 \times 10-2$a.u. (deepest red) and $6.409 \times 10-2$a.u. (deepest blue) in the maps, the most negative region on the MEP surface of the title compound is associated with the lone-pairs of the oxygen atom.

This indicates that the oxygen atom of this molecule is the most reactive site to interact favorably with an acidic reagent in the protonation reaction. The MEP analysis of the title compound, having a negative potential value -6.094×10^{-2}a.u. is concentrated on oxygen attached to thiophene ring and positive value of 6.094×10^{-2}a.u.

4.4. Atomic charge analysis

The Mulliken charge distributions of the molecule have been

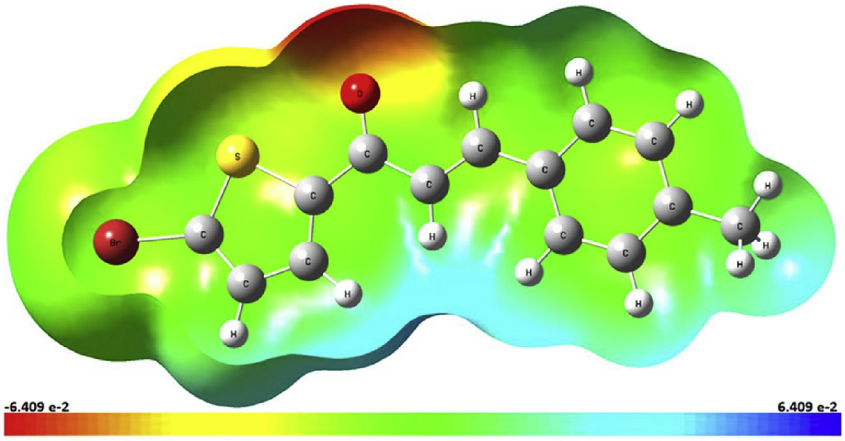

Fig. 9. MEP surface of the title compound.

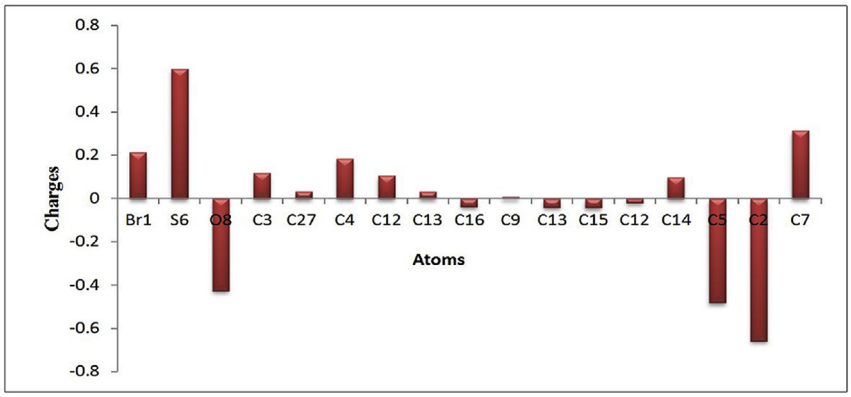

Fig. 10. The Mulliken atomic charges (except hydrogen) using B3LYP/6-31G(d).

Table 4
Static dipole moments μ(0; 0), polarizability [α(−ω; ω,0)] and first order hyperpolarizability [β(−ω; ω,0)] components of title molecule obtained with B3LYP/6-31Gd level.

Dipole moment (Debye)		Hyperpolarizability in esu ($\times 10^{-30}$)	
μ_x	−3.43	β_{xxx}	13.42
μ_y	−3.58	β_{yyy}	−0.12
μ_z	0.82	β_{zzz}	−0.01
μ_{tot}	5.03	β_{xxy}	10.95
μ_{urea}	4.72	β_{yyz}	0.81
Polarizability in esu ($\times 10^{-24}$)		β_{zzy}	0.14
α_{xx}	53.66	β_x	12.49
α_{yy}	22.2	β_y	10.69
α_{zz}	11.76	β_z	−0.37
$<\alpha>$	29.21	β-V	16.45
$<\alpha>_{urea}$	4.78	β-V_{urea}	0.31

calculated using B3LYP/6-31G(d) level [44]. The magnitude of the carbon Mulliken charges, found to be either positive or negative ranging from −0.6573 to 0.3141. The whole protons have a positive charge, while oxygen (O8 = −0.4265) atom has negative charge. The most positive charge is over sulfur (S6 = 0.6004) atom. The carbon atom bonded to sulfur and bromine has more negativity than other carbon atoms as shown in Fig. 10.

4.5. Computational NLO studies

The quantum chemical computational approach was used to calculate NLO properties such as dipole moment (μ), polarizability (α) and hyperpolarizabilities (β). The polarizability and hyperpolarizability components are the derivatives of molecular energy with respect to the strength of the applied electric field. The static hyperpolarizability, polarizability, and dipole moments of the title molecule were investigated using density function theory with B3LYP/6-31G(d) basis set. The dipole moment (μ), mean polarizability ($<\alpha>$), and first hyperpolarizability (β-V) were calculated using the following equations [45,46].

$$\mu = \left(\mu_x^2 + \mu_y^2 + \mu_z^2\right)$$

$$<\alpha> = \frac{1}{3}\left(\alpha_{xx} + \alpha_{yy} + \alpha_{zz}\right)$$

The magnitude of the total first order hyperpolarizability can be calculated using the following equation.

$$\beta_{tot} = \sqrt{\left(\beta_x^2 + \beta_y^2 + \beta_z^2\right)}$$

Where $\beta_x = \beta_{xxx} + \beta_{xyy} + \beta_{xzz}$; $\beta_y = \beta_{yyy} + \beta_{yzz} + \beta_{yxxz}$ and. $\beta_z = \beta_{zzz} + \beta_{zxx} + \beta_{zyy}$.

The first order polarizability (β) that is a third rank tensor that can be described by a $3 \times 3 \times 3$ matrix. According to Kleinman symmetry ($\beta_{xyx} = \beta_{xyy} = \beta_{yyx}$; $\beta_{yyz} = \beta_{yzy} = \beta_{zyy}$, …likewise other permutations also take same value), the 27 component of 3D matrix can be reduced to 10 components [47]. These components have been calculated using GAUSSIAN 09.

The obtained values were in atomic units (a.u.) and those values have been converted into standard units by making use of the conversion factors, for μ1 a. u. = 2.5412 Debye, for α1 a. u. = 0.1482×10^{-24} esu, and for β 1 a. u. = 8.6393×10^{-33} esu. The calculated values of the molecule are shown in Table 4.

It is found that the calculated the mean polarizability ($<\alpha>$) is 6 times higher than urea and the static β-V value for title molecule is 53 times higher than that of urea standard. Thus the title compound suggests that the molecule is a potential candidate for NLO application.

5. Conclusions

The crystal structure of (E)-1-(5-bromothiophen-2-yl)-3-(*p*-tolyl) prop-2-en-1-one compound was confirmed by single crystal X-ray diffraction. The compound crystallized in monoclinic crystal system with $P2_1/a$ space group, and the non-planarity was confirmed by dihedral angles between the thiophene and benzene rings is 41.61 (16) Å. The DFT optimized structure of the title compound shows a good agreement between the experimental and theoretical calculations using DFT with B3LYP/6-31G(d) level basis set. The Hirshfeld surface analysis and finger print plots were carried out to understand the molecular interactions. It was found that H···H (26.7%) and C···H (26.3%) interactions are major contributor in crystal packing. The MEP plots revealed the possible reactions sites of the molecule. The higher values of polarizability and first order hyperpolarizabilities of the title molecule suggest that the molecule is a potential candidate for NLO applications.

Acknowledgements

The authors are grateful to the National Single Crystal Diffractometer Facility, Department of Studies in Physics, University of Mysore, Manasagangotri, Mysuru, for providing X-ray diffractometer and computational facility. The authors are also thankful to

DST-FIST for providing financial support under research grant scheme SR/FST/ETT-378/2014.

References

[1] B. Deepa, P. Philominathan, Optik 127 (2016) 8698–8705.
[2] M. Rajkumar, A. Chandramohan, Mater. Lett. 181 (2016) 354–357.
[3] Ö. Tamer, D. Necmi, A. Davut, A. Yusuf, Ö.İ. İlhan, C. Mehmet, Spectrochim. Acta A 137 (2015) 1387–1396.
[4] F. Meyers, S.R. Marder, B.M. Pierce, J.L. Bredas, J. Am. Chem. Soc. 116 (1994) 10703–10714.
[5] H.K. Hsieh, T.H. Lee, J.P. Wang, J.J. Wang, C.N. Lin, Pharm. Res. 15 (1998) 39–46.
[6] S. Murakami, M. Muramatsu, H. Aihara, S. Otomo, Biochem. Pharmacol. 42 (1991) 1447–1451.
[7] M. Liu, P. Go, M.L. Wilairat, J. Med. Chem. 44 (2001) 4443–4452.
[8] A.A. Bekhit, N.S. Habib, A. Bekhit, Boll. Chim. Farm. 140 (2001) 297–301.
[9] H. Terashima, K. Hama, R. Yamamoto, M. Tsuboshima, R. Kikkawa, I. Hatanaka, Y. Shigeta, J. Pharmacol. Exp. Therapeut. 229 (1984) 226–230.
[10] T. Yoshioka, T. Fujita, T. Kanai, Y. Aizawa, T. Kurumada, K. Hasegawa, H. Horikoshi, J. Med. Chem. 32 (1989) 421–428.
[11] A.K. Singh, G. Saxena, R. Prasad, A. Kumar, J. Mol. Struct. 1017 (2012) 26–37.
[12] V. Shettigar, P.S. Patil, S. Naveen, M.A. Sridhar, S.M. Dharmaprakash, J. Shashidhara Prasad, J. Cryst. Growth 295 (2006) 44–49.
[13] F.Z. Henari, D. Gaynor, D.M. Griffith, C. Mulcahy, C.J. Marmion, Chem. Phys. Lett. 552 (2012) 126–129.
[14] C.P. Singh, R. Sharma, V. Shukla, P. Khundrakpam, R. Misra, K.S. Bindra, R. Chari, Chem. Phys. Lett. 616 (2014) 189–195.
[15] X. Fu, J. Feng, Z. Dong, L. Lin, X. Liu, X. Feng, Eur. J. Org Chem. 27 (2011) 5233–5236.
[16] M. Sharshira, N.M.M. Hamada, Am. J. Org. Chem. 2 (2012) 26–31.
[17] S. Czemmel, S.C. Heppel, J. Bogs, Protoplasma 249 (2012) 109–118.
[18] R.M. Wood, Springer Opt. Sci. 42 (2000) 423–424.
[19] J. Lin, R. Sa, M. Zhang, K. Wu, J. Phys. Chem. A 119 (2015) 8174–8181.
[20] F.D. Brunner, O.P. Kwon, S.J. Kwon, M. Jazbinsek, A. Schneider, P. Günter, Optic Express 16 (2008) 16496–16508.
[21] Z. Sun, S. Li, S. Zhang, F. Deng, M. Hong, J. Luo, Adv. Opt. Mater 2 (2014) 1199–1205.
[22] M.H. Youssoufi, P.K. Sahu, P.K. Sahu, D.D. Agarwal, M. Ahmad, M. Messali, S. Lahsasni, T.B. Hadda, Med. Chem. Res. 24 (2015) 2381–2392.
[23] P.J. Tejkiran, M.S. Brahmateja, P. Sai Siva Kumar, S. Pranitha, Philip Reji, S. Naveen, N.K. Lokanath, S. Prathap Chandran, G. Nageswara Rao, J. Pho. Chem. Pho. Bio. A: Inside Chem. 324 (2016) 33–39.
[24] S. Naveen, J. Jamalis, Ming Liew Suk, C.S. Anandakumar, N.K. Lokanath, Chem. Data Coll. 7–8 (2016) 58–67.
[25] M.G. Prabhudeva, S. Bharath, A. Dileep Kumar, S. Naveen, N.K. Lokanath, B.N. Mylarappa, K. Ajay Kumar, Bioorg. Chem. 73 (2017) 109–120.
[26] N. Panigrahi, S. Ganguly, J. Panda, Y. Praharsha, Chem. Sci. Trans. 3 (2014) 1163–1171.
[27] Rigaku, NUMABS, Rigaku Corporation, Tokyo, Japan, 1999.
[28] Rigaku, CrystalClear, Rigaku Corporation, Tokyo, Japan, 2011.
[29] G.M. Sheldrick, Acta Crystallogr. C71 (2015) 3–8.
[30] A.L. Spek, Acta Crystallogr. A46 (1990) c34–c34.
[31] C.F. Macrae, I.J. Bruno, J.A. Chisholm, P.R. Edgington, P. McCabe, E. Pidcock, L.M. Rodriguez, R. Taylor, J. van de Streek, P.A. Wood, J. Appl. Crystallogr. 41 (2008) 466–470.
[32] M.J. Frisch, G.W. Trucks, H.B. Schlegel, G.E. Scuseria, M.A. Robb, J.R. Cheeseman, G. Scalmani, V. Barone, B. Mennucci, G.A. Petersson, H. Nakatsuji, M. Caricato, X. Li, H.P. Hratchian, A.F. Izmaylov, J. Bloino, G. Zheng, J.L. Sonnenberg, M. Hada, M. Ehara, K. Toyota, R. Fukuda, J. Hasegawa, M. Ishida, T. Nakajima, Y. Honda, O. Kitao, H. Nakai, T. Vreven, J.A. Montgomery, J.E. Peralta, F. Ogliaro, M. Bearpark, J.J. Heyd, E. Brothers, K.N. Kudin, V.N. Staroverov, R. Kobayashi, J. Normand, K. Raghavachari, A. Rendell, J.C. Burant, S.S. Iyengar, J. Tomasi, M. Cossi, N. Rega, J.M. Millam, M. Klene, J.E. Knox, J.B. Cross, V. Bakken, C. Adamo, J. Jaramillo, R. Gomperts, R.E. Stratmann, O. Yazyev, A.J. Austin, R. Cammi, C. Pomelli, J.W. Ochterski, R.L. Martin, K. Morokuma, V.G. Zakrzewski, G.A. Voth, P. Salvador, J.J. Dannenberg, S. Dapprich, A.D. Daniels, Ö. Farkas, J.B. Foresman, J.V. Ortiz, J. Cioslowski, D.J. Fox, Gaussian 09, Revision B.01, Wallingford CT, 2009.
[33] R. Dennington, T. Keith, J. Millam, GaussView, Semichem Inc., Shawnee Mission, KS, 2009, Version 05. .
[34] D.J.G.S.K. Wolff, J.J. McKinnon, M.J. Turner, D. Jayatilaka, M.A. Spackman, Crystal Explorer, 2012, Version3.1. .
[35] A.A. Prasad, K. Muthu, V. Meenatchi, M. Rajasekar, R. Agilandeshwari, K. Meena, J.V. Manonmoni, S.P. Meenakshisundaram, Spectrochim. Acta 140A (2015) 311–327.
[36] M. Aires-de-Sousa, M.C. Hemmer, J. Gasteiger, Anal. Chem. 74 (2002) 80–90.
[37] T. Samanta, L. Dey, J. Dinda, S.K. Chattopadhyay, S.K. Seth, J. Mol. Struct. 1068 (2014) 58–70.
[38] J.J. Koenderink, A.J. van Doorn, Image Vis Comput. 10 (1992) 557–564.
[39] S. Sherzaman, M.N. Ahmed, B.A. Khan, T. Mahmood, K. Ayub, M.N. Tahir, J. Mol. Struct. 1148 (2017) 388–396.
[40] M.D. Esrafili, Comput. Theor. Chem. 1015 (2013) 1–7.
[41] M.D. Esrafili, F. Mohammadian-Sabet, Chem. Phys. Lett. 628 (2015) 71–75.
[42] L. Szabo, V. Chiş, A. Pirnau, N. Leopold, O. Cozar, S. Orosz, J. Mol. Struct. 24 (2009) 385–392.
[43] M. Bartošková, Z. Friedl, Cent. Eur. J. Energy Mater 10 (2013) 103–112.
[44] R.S. Mulliken, J. Chem. Phys. 23 (1955) 1833–1840.
[45] H.A. Kurtz, J.J.P. Stewart, K.M. Dieter, J. Comput. Chem. 11 (1990) 82–87.
[46] G. Maroulis, J. Chem. Phys. 94 (1991) 1182–1190.
[47] R. Wortmann, P. Krämer, C. Glania, S. Lebus, N. Detzer, J. Chem. Phys. 173 (1993) 99–108.